The X-ray reflector in NGC 4945: A time-and space-resolved portrait

Monthly Notices of the ROYAL ASTRONOMICAL SOCIETY LETTERS

Mon. Not. R. Astron. Soc. (2012) doi:10.1111/j.1745-3933.2012.01232.x

The X-ray reflector in NGC 4945: a time- and space-resolved portrait

A. Marinucci,[1,2⋆] G. Risaliti,[2,3] Junfeng Wang,[2] E. Nardini,[2] M. Elvis,[2] G. Fabbiano,[2] S. Bianchi[1] and G. Matt[1]

[1]*Dipartimento di Fisica, Università degli Studi Roma Tre, via della Vasca Navale 84, 00146 Roma, Italy*
[2]*Harvard–Smithsonian Center for Astrophysics, 60 Garden Street, Cambridge, MA 02138, USA*
[3]*INAF - Osservatorio Astrofisico di Arcetri, Largo E. Fermi 5, 50125 Firenze, Italy*

Accepted 2012 February 6. Received 2012 February 6; in original form 2011 December 28

ABSTRACT

We present a time, spectral and imaging analysis of the X-ray reflector in NGC 4945, which reveals its geometrical and physical structure with unprecedented detail. NGC 4945 hosts one of the brightest AGN in the sky above 10 keV, but it is only visible through its reflected/scattered emission below 10 keV, due to absorption by a column density of $\sim 4 \times 10^{24}$ cm^{-2}. A new *Suzaku* campaign of five observations spanning ∼6 months, together with past *XMM–Newton* and *Chandra* observations, shows a remarkable constancy (within <10 per cent) of the reflected component. Instead, *Swift*-BAT reveals strong intrinsic variability on time-scales longer than 1 yr. Modelling the circumnuclear gas as a thin cylinder with the axis on the plane of the sky, we show that the reflector is at a distance ≥30–50 pc, well within the imaging capabilities of *Chandra* at the distance of NGC 4945 (1 arcsec ∼18 pc). Accordingly, the *Chandra* imaging reveals a resolved, flattened, ∼150 pc long clumpy structure, whose spectrum is fully due to cold reflection of the primary AGN emission. The clumpiness may explain the small covering factor derived from the spectral and variability properties.

Key words: accretion, accretion discs – galaxies: active – galaxies: Seyfert.

1 INTRODUCTION

NGC 4945 is an almost edge-on (inclination angle ∼80°) spiral galaxy hosting one of the nearest AGN ($D \sim 3.7$ Mpc, 1 arcsec = 18 pc; Mauersberger et al. 1996). NGC 4945 has been widely studied in the past, both in the soft and in the hard X-rays. It is the brightest Seyfert 2 and the second brightest radio-quiet AGN after NGC 4151 in the 100-keV sky (Done, Madejski & Smith 1996), with a strongly absorbed ($N_{\rm H} \sim 4 \times 10^{24}$ cm^{-2}; Itoh et al. 2008) intrinsic nuclear continuum, known to be extremely variable (Guainazzi et al. 2000; Madejski et al. 2000). Such a high column density completely blocks the primary nuclear emission below 8–10 keV, while the emission at higher energy is still visible, though heavily affected by Compton scattering and photoelectric absorption. A detailed analysis of the high-energy variability (Madejski et al. 2000; Done et al. 2003, hereafter D03) already provided important (and, so far, almost unique) constraints on the geometry of the reflector: the variability above 10 keV implies that most of the observed emission is due to the primary emission, and not to Compton scattering from other directions (which would dilute the intrinsic variability, producing an almost constant observed emission). This, in turn, means that the reflector covers a solid angle <10° as seen from the source (assuming a toroidal structure). This is also in agreement with the unusually low ratio between the observed, reflected emission below 10 keV and the intrinsic flux in the same band as estimated from the emission above 10 keV ($f < 0.1$ per cent). Finally, a *Chandra* observation revealed a spatially resolved component, on a ∼100 pc scale, whose spectrum is typical of Compton reflection from a ∼neutral medium (D03).

Here we present the analysis of new and archival *Suzaku*, *XMM–Newton* and *Chandra* observations, focusing specifically on the determination, with unprecedented detail, of the dimensions and the geometrical structure of the circumnuclear absorber/reflector in NGC 4945. A complete study, discussing both the *Chandra* imaging data and our new *Suzaku* observations, will be presented in a separate paper (Marinucci et al. 2012, in preparation). The work presented here expands the results summarized above, through two completely new studies: (i) the comparison between the intrinsic variability *above* 10 keV (from *Swift*-BAT observations) and the reflection variability *below* 10 keV (from a set of eight *XMM–Newton* and *Suzaku* observations over a period of ∼10 years); (ii) a detailed analysis of the spatial extension of the reflector, taking advantage

⋆E-mail: marinucci@fis.uniroma3.it

of the full set of available *Chandra* observations, is discussed in the next sections.

2 OBSERVATIONS AND DATA REDUCTION

Chandra. NGC 4945 was observed by *Chandra* on 2000 January 27–28 for a total exposure time of 49 ks, with the ACIS camera. It was observed again 4 years later twice, for a total exposure time of 180 ks, taking advantage of the HETG instrument. Data were reduced with the CIAO 4.3 package (Fruscione et al. 2006) and using the Chandra Calibration Data Base (CALDB) version 4.4.6, adopting standard procedures. The imaging analysis was performed on a file including the two merged HETG zeroth-order images re-projected on the ACIS-S image, applying the SER and smoothing procedures widely discussed in the literature (Tsunemi et al. 2001; Li et al. 2004; Wang et al. 2011). We therefore use a pixel size of 0.246 arcsec in Fig. 2 and 0.123 arcsec in Fig. 4. After cleaning for background flaring, we get a total of 34 and 173 ks for the 2000 and the 2004 HETG zeroth-order merged observations, respectively. Spectra were extracted on both the data set from three different regions: a circle with 25-arcsec radius (matching the *XMM–Newton* extraction region, see below); a $12 \times 6\,\mathrm{arcsec}^2$ box and a central circle with 1.5-arcsec radius. We grouped all extracted spectra to have at least 20 total counts per new bin.

Suzaku. The six *Suzaku* observations analysed in this Letter were performed with the X-ray Imaging Spectrometer (XIS). The first one has been performed in 2006, has a duration of ∼100 ks and has been presented by Itoh et al. (2008). The remaining five observations, with a duration of 40 ks each, have been performed between 2010 July and 2011 January, as part of a monitoring campaign of this source.

The event files were processed and calibrated adopting standard procedures, discussed in several previous papers (e.g. Maiolino et al. 2010). The source extraction radius is 1.85 arcmin for all the six observations. Background spectra have been extracted from source-free regions with 3-arcmin radii. The 0.5–10 keV spectra extracted from the front-illuminated XIS0 and XIS3 have been co-added.

XMM–Newton. We used two *XMM–Newton* observations performed with the EPIC-PN camera operated in large window and medium filter modes. Source data 'cleaning' (exclusion of flaring particle background intervals) was performed with SAS 10.0.0 (Gabriel et al. 2004) via an iterative process which leads to a maximization of the signal-to-noise ratio (S/N), similarly to that described in Piconcelli et al. (2004). Source spectra were extracted from a 25-arcsec radius circle; background spectra were extracted from source-free circular regions of the source field.

Swift. The *Swift*-BAT 15–195 keV light curve has been obtained from the online catalogue[1] which at the time of our analysis was available for 65 months.

3 THE REFLECTOR GEOMETRY FROM TIME AND SPECTRAL VARIABILITY

NGC 4945 offers a *unique* possibility to perform a comparison between the variability of the intrinsic and the reflected X-ray emission, because it is the only known AGN with both (i) Compton thickness $\tau_C > 1$ and (ii) a strong intrinsic variability above 10 keV. For *all* the other known bright AGN, such a detailed direct comparison between the variabilities of the two components is impossible because one of the two above mentioned conditions is not satisfied.

(i) If the AGN is not Compton-thick, the Compton reflection component is diluted by the dominant direct component. The separation of the two components is never precise, and typical uncertainties in the flux of the reflected component are of the order of 20–30 per cent even for long observations of the brightest AGN.

(ii) The AGN is Compton-thick, but the intrinsic emission is either not visible (due to $N_H > 10^{25}\,\mathrm{cm}^{-2}$, as in NGC 1068) or, anyway, not variable, probably because of the dilution due to multiple Compton scatterings (such as in the Circinus galaxy).

NGC 4945 shows one of the brightest reflection dominated spectra below 10 keV, with flux measurement uncertainties of the order of ∼1 per cent, and a high-quality light curve of its intrinsic emission above 10 keV, provided by *Swift*-BAT. The highest quality spectra below 10 keV have been obtained in the eight *XMM–Newton* and *Suzaku* observations presented in the previous section.

The 3–10 keV spectra of these observations have been fitted with a model consisting of a reflection continuum (PEXRAV; Magdziarz & Zdziarski 1995), three emission lines for neutral, He-like and H-like iron, and an additional power law, requested by the fit, and associated with the diffuse emission (see below). From the analysis of the HETG grating spectra, we rule out the presence of emission features associated with the iron Kβ line. The analysis has been performed with the XSPEC 12.7 code (Arnaud et al. 1996). All quoted errors are at the 90 per cent confidence level for one interesting parameter. This model successfully reproduces all the individual spectra, with best-fitting parameters typical of reflection-dominated sources. The details of the spectral model have been discussed in Itoh et al. (2008), Schurch, Roberts & Warwick (2002) and D03, and will be further analysed in a forthcoming paper, together with the soft emission. What is interesting in this context is instead the possible variability of the reflected component. In this respect, the following results are relevant.

(1) The analysis of the *Chandra* spectrum of the resolved $12 \times 6\,\mathrm{arcsec}^2$ box shows that the central emission is well fitted by a pure reflection continuum, with no need for an additional power law, so confirming that this component is needed only to reproduce the circumnuclear emission. Similarly, the *XMM–Newton* spectrum, extracted from the central 25 arcsec, requires only a minor contribution from the additional power law (about 1/10 of that in the *Suzaku* spectra).

(2) If we fit the eight spectra with constant reflection component and emission lines, leaving the additional power law as the only variable component, we obtain an equally good fit, with no significant residuals in any individual spectrum. This implies that formally *all* the observed variability may be due to galactic sources.

(3) The whole luminosity within the central 1.85-arcmin region is only $\sim 2 \times 10^{39}\,\mathrm{erg\,s}^{-1}$. It is therefore not surprising if significant variability due to single sources is observed.

Based on the above considerations, we conclude that the best way to estimate the reflection variability is to fit the eight spectra with the model described above, with only three free parameters: the slope and the normalization of the additional power law, and the flux F of the reflection (continuum plus lines) component, normalized to the value of the first interval, for ease of comparison. The results are reported in Table 1 and show no significant variability in any observation. If we assume a constant value of the relative flux F, we obtain $\langle F \rangle = 0.98 \pm 0.02$ and a marginally better fit

[1] http://swift.gsfc.nasa.gov/docs/swift/results/bs58mon/

Table 1. Best-fitting values for the reflection component.

Param.	Value	OBS	Date	F^e
Γ	1.6 ± 0.1	*Suzaku* 1	01/06	1.00 ± 0.06
E(1)[a]	6.39 ± 0.01	*Suzaku* 2	07/10	1.00 ± 0.08
EW(1)[b]	1020 ± 100	*Suzaku* 3	07/10	0.99 ± 0.08
E(2)[a]	6.66 ± 0.01	*Suzaku* 4	07/10	0.97 ± 0.08
EW(2)[b]	130 ± 20	*Suzaku* 5	08/10	0.98 ± 0.08
E(3)[a]	7.02 ± 0.01	*Suzaku* 6	01/11	0.94 ± 0.08
EW(3)[b]	140^{+20}_{-10}	*XMM* 1	01/00	0.97 ± 0.05
N^c	3.7 ± 0.7	*XMM* 2	01/04	0.98 ± 0.06
F_{2-10} [d]	1.3×10^{-12}	*Chandra* 25″	05/04	1.08 ± 0.11
L_{2-10} [d]	2.2×10^{39}	*Chandra* BOX	05/04	0.86 ± 0.07
χ^2/d.o.f.	1308/1205	*Chandra* 1.″5	05/04	0.58 ± 0.06

[a]Emission line energies, in keV; [b]line equivalent widths, in eV; [c]normalization in units of 10^{-3} ph cm^{-2} s^{-1} keV^{-1}; [d]2–10 keV flux and luminosity of the reflection spectrum, in cgs units; [e]relative flux.

(the χ^2 increases by 3, with seven more degrees of freedom). The dispersion around the central value is significantly smaller than the uncertainties on the individual values. This is due to the partial degeneracy among the spectral parameters. Based on these results, we estimate an upper limit to the observed reflection variability of ∼4 per cent, corresponding to twice the dispersion or, equivalently, to the ratio between the maximum and minimum value of F within the measured dispersion. This result can be compared with the variability observed at higher energies. The average 15–150 keV flux of NGC 4945 is of the order of 5–10 mcrab, therefore the *Swift*-BAT monitoring provides reliable, high S/N light curves with reasonably short time bins. In Fig. 1 we show the 65-month light curve, in bins of 1 and 5 months. In order to obtain a semi-quantitative estimate of the reflector distance, we modelled the circumnuclear gas as a cylinder with the axis on the plane of the sky, with radius R and height H, such that $H/R < 0.1$, as implied by the analysis of D03. We then used the observed BAT light curve as an input, and determined the maximum observable flux variation of the reflected component as a function of the distance R, by adding the contribution of each element of the reflector. Qualitatively, we expect that the more distant the reflector, the lower variability is observed in the reflected light curve, because the intrinsic variability is smoothed out by the different lengths of the light paths corresponding to each reflecting element. Quantitatively, the result is shown in Fig. 1 (lower panel). In order to observe a variation not larger than 4 per cent (reminding that $\langle F \rangle = 0.96$–1.00), the reflector must be at a distance larger than 35 pc. This result is obviously approximate, due to the assumptions on the geometry and to the limited sampling of the reflection fluxes, which may have caught the source in the same reflected states by chance. However, we believe it provides a solid order of magnitude estimate of the distance of the reflector. We conclude noting that, considering that the *Chandra* resolution is ∼0.25 arcsec, (∼5 pc at the distance of NGC 4945), the X-ray reflector should be easily resolved by *Chandra*, consistent with the conclusions of D03.

4 THE REFLECTOR GEOMETRY FROM DIRECT IMAGING

In Fig. 2 the 1×1 arcmin^2 central region of NGC 4945 is shown. After running the script CHANDRA_REPRO on the three *Chandra* event files, we merged them all with the MERGE_ALL script and filtered them in energy between 0.3–2 keV (in red) and 2–10 keV (in green). A soft X-ray emitter can be seen in the top-right region of the

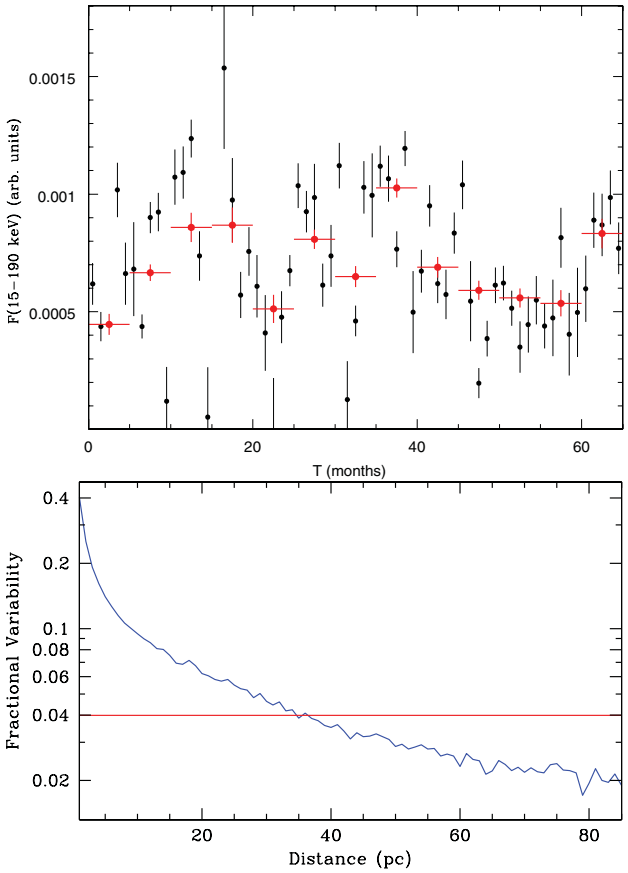

Figure 1. Upper panel: *Swift*-BAT light curve of the 15–195 keV emission of NGC 4945, grouped in time bins of 1 month (black) and 5 months (red). Lower panel: expected maximum variability as a response of a cylindrical reflector to the BAT light curve, as a function of the distance from the central source. The value corresponding to the upper limit to the observed reflection variability is ∼35 pc.

image, as already discussed in Schurch et al. (2002), where they called it the 'plume', reproduced by a single temperature thermal model ($kT \sim 0.6$ keV), interpreted as a mass-loaded superwind emanated from the central nuclear starburst. With the inclusion of the two 2004 observations in the image, we notice a further soft lobe in the bottom-left direction indicating a second, possible emitter partially absorbed by a dust-lane crossing the nucleus, aligned with the clumpy structure shown in Fig. 4. For this analysis, we refer to a future work (Marinucci et al., in preparation).

The nuclear 2–10 keV emission is embedded in a 12×6 arcsec^2 box, corresponding to a 180×90 pc region, which is consistent with the starburst ring traced by molecular gas (Moorwood et al. 1996; Marconi et al. 2000; Curran et al. 2001).

We performed a spectral analysis of three zones, corresponding to the *XMM–Newton* extraction region, a 12×6 arcsec^2 box, including most of the hard emission (Fig. 2), and a central circular region with radius 1.5 arcsec. The spectra, shown in Fig. 3, are fitted with the same reflection model as described above, with a contribution of the additional power law decreasing from the larger to the small region. In particular, (i) the best fitting model of the spectrum from the 25-arcsec circle is fully consistent (in each individual parameter) with that of the *XMM–Newton* observations, (ii) the spectrum from the 12×6 arcsec^2 box is again fitted with the same model, but with a relative flux of the reflection component $F = 0.86 \pm 0.07$, indicating that most of the reflection comes from this region, with

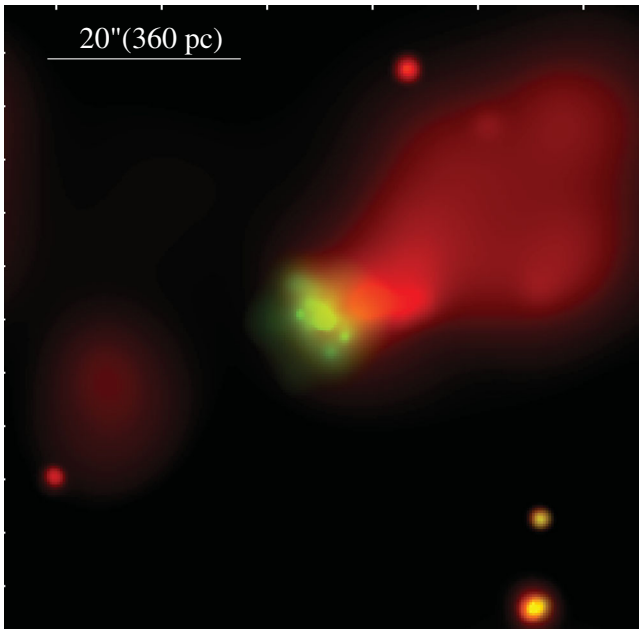

Figure 2. Two-colour (red: 0.3–2 keV; green: 2–10 keV) *Chandra* image of the 1 × 1 arcmin^2 central region of NGC 4945.

only a remaining ∼10 per cent from outer regions, (iii) the model from the central annulus is fitted with a pure reflection component, with no need for the additional power law. The relative flux is $F = 0.58 \pm 0.06$. This shows that the reflection emission is moderately concentrated in the projected central ∼30 pc, but with a significant contribution from the outer regions. In our simple cylindrical scheme, if a small (a few degrees) inclination angle is assumed, this concentration in the central unresolved region is expected due to the projection effect and is not related to a small physical distance from the X-ray source. A direct, complementary way to demonstrate that the hard X-ray emission is dominated by the reflected, diffuse component is by comparing the image in the full hard X-ray spectral interval (2–10 keV), with the exclusion of the 6.2–6.7 energy range, with the 'iron line image' obtained filtering only the 6.2–6.7 keV spectral interval (Fig. 4), which is clearly dominated by the iron emission line (Fig. 3). We then superimposed the contours of the hard X-rays on the iron Kα emitter. The striking match between these two images demonstrates that the cold reflection and the iron emission lines originate exactly from the same circumnuclear material and we are actually able to take a screenshot of the inner reflecting structure of NGC 4945.

Finally, we notice that the emission in Fig. 4 originates from a non-homogeneous structure, with visible clumps and empty regions with sizes of the order of tens of parsecs. The differences in counts among these subregions are highly significant (same area regions of 10 × 10 pixels contain from <10 to > 100 counts). A smaller scale clumpiness of these structures, not resolved by *Chandra*, may explain the low covering factor (<10 per cent) of the reflector, as estimated from the high intrinsic variability above 10 keV, and from the low ratio between the reflected and intrinsic components (Madejski et al. 2000).

5 CONCLUSIONS

The time, spectral and imaging analysis of the X-ray emission of NGC 4945 based on *XMM–Newton*, *Suzaku*, *Swift*-BAT and

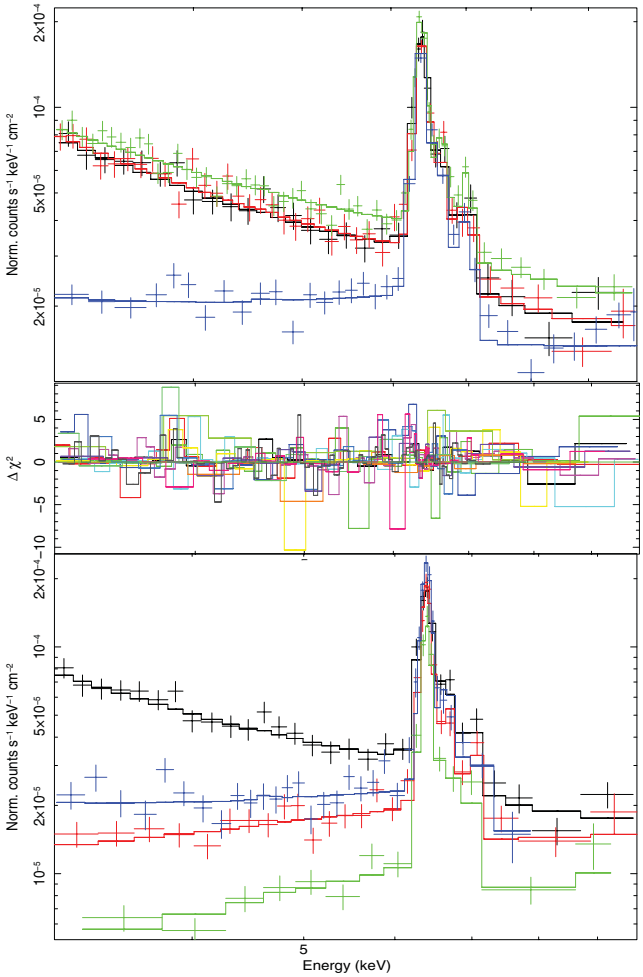

Figure 3. Spectra (rescaled to a common effective area), model and $\Delta\chi^2$ from the observations. The $\Delta\chi^2$ values are shown for all the spectra in the central panel, while only some of the spectra are shown, for clarity. Upper panel: first *Suzaku* observation in 2010 (black); *Suzaku* in 2011 (red); *Suzaku* in 2006 (green); *XMM–Newton* in 2004 (blue). Lower panel: the first 2010 *Suzaku* observation is shown again (black) for ease of comparison; the remaining spectra are from the *Chandra* 2004 data, extracted from a 25-arcsec radius, (blue) a 12 × 6 arcsec^2 box (red) and a 1.5-arcsec radius circle (green). It is worth noting that the spectra between 6 and 7 keV, dominated by the iron line emission, are almost identical in all observations, except for the last one from *Chandra*, and that the total continuum decreases with the area of the extraction region. Both these features are evidence that the variability is due to the diffuse galactic component, while the reflection remains constant, as quantitatively demonstrated by the spectral fits (Table 1).

Chandra data characterizes the AGN circumnuclear reflector with unprecedented detail.

(1) The comparison between the strong intrinsic variability measured by *Swift*-BAT and the constant reflection spectra from *XMM–Newton* and *Suzaku* observations over more than 10 years implies a distance of the reflector $D > 35$ pc.

(2) The *Chandra* image, obtained combining two observations performed in 2000 and 2004, reveals an extended hard emission on projected scales of ∼200 × 100 pc. The spectrum of this emission is entirely reproduced by a cold reflection model. The central 30 pc accounts for about 50 per cent of the whole emission.

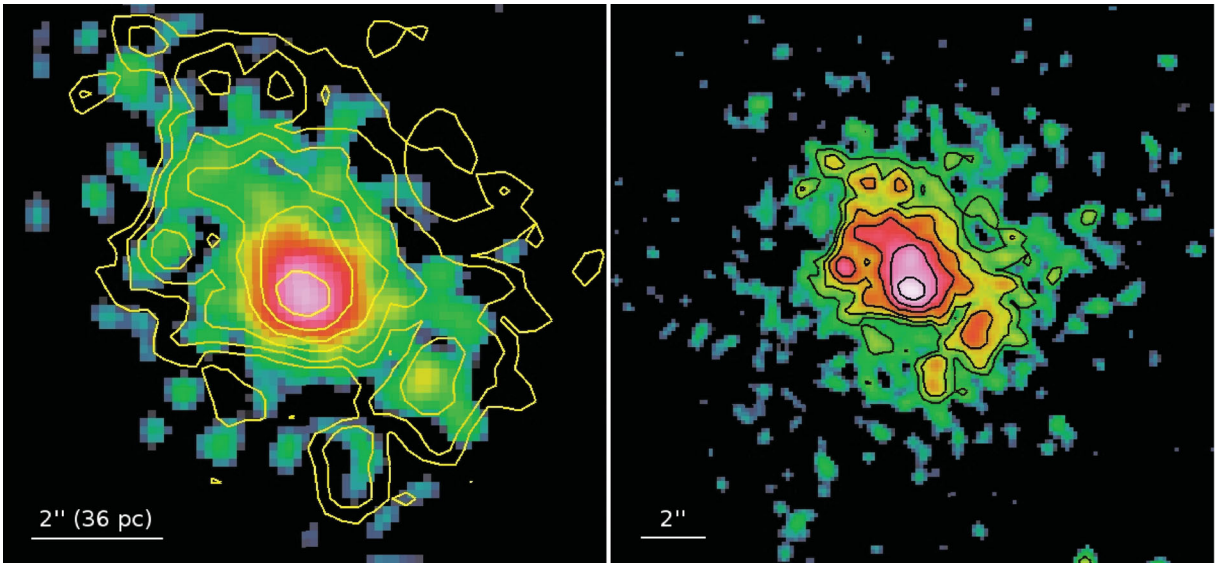

Figure 4. Image of the central region in the line emission band (6.2–6.7 keV, left) and in the hard X-ray band (right).

(3) We show the first X-ray image of the inner reflector of an AGN. The large-scale structure of the emission region is clumpy and asymmetric, and the central region is resolved by *Chandra*. A smaller scale, unresolved clumpiness may explain the low covering factor of the reflector inferred by the high variability of the intrinsic emission at $E > 10$ keV, and by the low ratio between reflected and intrinsic spectrum (Madejski et al. 2000; D03).

ACKNOWLEDGMENTS

The authors are grateful to the referee for her/his useful comments. AM, GR and EM acknowledge NASA grants NNX11AC85G and NNX10AF50G. JW acknowledges support from NASA grants GO8-9101X and GO1-12009X.

REFERENCES

Arnaud K. A., 1996, in Jacoby G., Barnes J., eds, ASP Conf. Ser. Vol. 101, Astronomical Data Analysis Software and Systems V. Astron. Soc. Pac., San Francisco, p. 17
Curran S. J., Johansson L. E. B., Bergman P., Heikkilä A., Aalto S., 2001, A&A, 367, 457
Done C., Madejski G. M., Smith D. A., 1996, ApJ, 463, L63
Done C., Madejski G. M., Życki P. T., Greenhill L. J., 2003, ApJ, 588, 763 (D03)
Fruscione A. et al., 2006, SPIE, 6270, 62701V
Gabriel C. et al., 2004, in ASP Conf. Ser. Vol. 314, Astron. Soc. Pac., San Francisco, p. 759
Guainazzi M., Matt G., Brandt W. N., Antonelli L. A., Barr P., Ba ssani L., 2000, A&A, 356, 463
Itoh T. et al., 2008, PASJ, 60, 251
Li J., Kastner J. H., Prigozhin G. Y., Schulz N. S., Feigelson E. D., Getman K. V., 2004, ApJ, 610, 1204
Madejski G., Życki P., Done C., Valinia A., Blanco P., Rothschild R., Turek B., 2000, ApJ, 535, L87
Magdziarz P., Zdziarski A. A., 1995, MNRAS, 273, 837
Maiolino R. et al., 2010, A&A, 517, A47
Marconi A., Oliva E., van der Werf P. P., Maiolino R., Schreier E. J., Macchetto F., Moorwood A. F. M., 2000, A&A, 357, 24
Mauersberger R., Henkel C., Whiteoak J. B., Chin Y.-N., Tieftrunk A. R., 1996, A&A, 309, 705
Moorwood A. F. M., van der Werf P. P., Kotilainen J. K., Marconi A., Oliva E., 1996, A&A, 308, L1
Piconcelli E., Jimenez-Bailón E., Guainazzi M., Schartel N., Rodríguez-Pascual P. M., Santos-Lleó M., 2004, MNRAS, 351, 161
Schurch N. J., Roberts T. P., Warwick R. S., 2002, MNRAS, 335, 241
Tsunemi H., Mori K., Miyata E., Baluta C., Burrows D. N., Garmire G. P., Chartas G., 2001, ApJ, 554, 496
Wang J. et al., 2011, ApJ, 742, 23

This paper has been typeset from a TEX/LATEX file prepared by the author.